© Pol J Radiol 2022; 87: e246-e256
DOI: https://doi.org/10.5114/pjr.2022.116167

Received: 24.04.2021
Accepted: 17.05.2021
Published: 06.05.2022

Polish Journal of Radiology

http://www.polradiol.com

Original paper

Intravoxel incoherent motion diffusion-weighted imaging (IVIM-DWI) of the major salivary glands: an assessment of the optimal number and combination of *b*-values

Mitsuhiro Kimura[1,A,B,C,D,E,F], Hidetake Yabuuchi[1,A,B,D,E], Hiroshi Narita[2,B,D], Yoichi Kurihara[3,B], Kiyoshi Hisada[3,B], Noriyuki Sakai[1,D], Kazuya Nagatomo[1,D], Ryoji Mikayama[1,D], Masafumi Masaki[3,B], Hiroshi Kimura[4,B]

[1]Department of Health Sciences, Graduate School of Medical Sciences, Kyushu University, Fukuoka, Japan
[2]Hitachi, Ltd., Tokyo, Japan
[3]Department of Radiology, Kimura Hospital, Fukuoka, Japan
[4]Department of Surgery, Kimura Hospital, Fukuoka, Japan

Abstract

Purpose: To examine the optimal number and combination of *b*-values in intravoxel incoherent motion (IVIM) diffusion-weighted imaging (DWI) of the major salivary glands.

Material and methods: IVIM-DWI was performed on 10 healthy volunteers using 13 *b*-values (low *b*-values: 0-100 s/mm^2; high *b*-values: 200-1000 s/mm^2). The IVIM parameters and apparent diffusion coefficient of the bilateral major salivary glands were calculated using 13 *b*-values and were considered the standard values. We sequentially reduced the number of *b*-values to 10, 8, 6, and 5. The parameters in each combination were calculated. The standard values were compared with the parameters from each reduced *b*-value in IVIM-DWI. The Wilcoxon signed-rank test was used to determine whether there were any differences between the parameters in each combination. Bonferroni correction was conducted for multiple comparisons.

Results: There were no significant differences between the standard values and parameters from the 2 combinations of 6 *b*-values. However, significant differences were observed between the standard values and parameters from some combinations of only 2 low or only 2 high *b*-values.

Conclusions: IVIM-DWI of the major salivary glands could be performed using a minimum of 6 *b*-values. However, they should contain 3 low and 3 high *b*-values.

Key words: salivary glands, magnetic resonance imaging, diffusion, perfusion, quantitative evaluation.

Introduction

Intravoxel incoherent motion (IVIM) involves the diffusion of water molecules and perfusion [1,2]. Diffusion-weighted imaging (DWI) is used to evaluate IVIM. However, the diffusion of water molecules alone can be evaluated through DWI using high *b*-values to exclude perfusion. Le Bihan proposed the use of IVIM-DWI, which could assess the diffusion of water molecules and perfusion separately [2].

The apparent diffusion coefficient (ADC) is generally used as the quantitative parameter in DWI. In IVIM-DWI, the diffusion of water molecules and perfusion are evaluated using the following parameters: perfusion fraction (f [%]), diffusion coefficient (D [mm^2/s]), and

Correspondence address:
Mitsuhiro Kimura, Department of Health Sciences, Graduate School of Medical Sciences, Kyushu University, Fukuoka, Japan,
e-mail: mitsuhirokimura0426@gmail.com

Authors' contribution:
A Study design · **B** Data collection · **C** Statistical analysis · **D** Data interpretation · **E** Manuscript preparation · **F** Literature search · **G** Funds collection

pseudo-diffusion coefficient (D × [mm²/s]). The IVIM parameters were calculated using the following equation:

$$S_b/S_0 = (1 - f) \times \exp(-bD) + f \times \exp[-b \times (D + D^*)] \quad (1)$$

where S_b is the signal intensity at a *b*-value greater than 0 s/mm² and S_0 is the signal intensity at a *b*-value of 0 s/mm². Equation (1) shows a bi-exponential function, and a bi-exponential curve fitting is performed on the graph of Equation (1). Thus, multiple *b*-values are required to obtain IVIM parameters. IVIM-DWI using a large number of *b*-values can accurately estimate IVIM parameters. However, this method is disadvantageous because it has a long imaging time [3]. The *b*-values in IVIM-DWI in individuals with kidney [4], prostate [5], and breast cancers [6] have been evaluated. Previous studies have reported that the required number of *b*-values in IVIM-DWI of the abdomen is more than 10 [3], and more than 2 *b*-values between 0 and 50 s/mm² are required in IVIM-DWI of the liver [7]. Furthermore, 4 optimised *b*-values can be used for the assessment of IVIM parameters in liver lesions [8].

Some studies have reported the utility of IVIM-DWI in patients with salivary gland tumours, pharyngeal cancer, laryngeal cancer, and lymph node metastasis in the head and neck [9-18]. However, there has been no report on the optimal number and combination of *b*-values in IVIM-DWI of major salivary glands, and the optimum settings of *b*-values in that must be investigated to maintain the quality in the assessment of each parameter and shorten the imaging time.

Thus, the current study aimed to examine the optimal number and combination of *b*-values in IVIM-DWI of the major salivary glands.

Material and methods

Participants

This study was approved by our institutional review board, and written informed consent was obtained from all participants. Ten healthy volunteers (4 men and 6 women, with an average age of 21.7 [range: 21-24] years) were enrolled in this study.

Magnetic resonance imaging

All healthy volunteers underwent MRI using a 1.5-T machine (Echelon Vega, Hitachi, Ltd., Tokyo, Japan) with a 16-channel head coil. Magnetic resonance imaging (MRI) was performed using multi-shot spin echo-echo planar imaging (EPI) with 2 shots and 13 *b*-values (low *b*-values: 0, 10, 20, 30, 40, 50, 75, and 100 s/mm²; high *b*-values: 200, 300, 500, 750, and 1000 s/mm²). Low and high *b*-values were distinguished by a *b*-value of 200 s/mm² because the influence of perfusion was almost excluded using *b*-values larger than 200 s/mm². The following parameters were used: repetition time/echo time, 3300/62.4 ms; field of view, 230 × 230 mm²; matrix size, 136 × 192; thickness/gap, 5.0/0.5 mm; number of signal averages, 2; sensitivity encoding factor, 2; fat saturation, chemical shift selective; and bandwidth, 250 kHz. Intervals of motion probing gradient (MPG) pulses (Δ) were 30.724 ms, and the duration of each MPG pulse (δ) was 21.056 ms. The scanning time was 12 min and 21 s. Before every acquisition of IVIM-DWI, calibration scans to predict and correct the eddy current caused by MPG pulses were performed.

Calculation of the IVIM parameters and ADC

The influence of D* can be neglected when *b*-values larger than 200 s/mm² were used. Thus, Equation (1) on this condition can be simplified as follows:

$$S_{b1}/S_{b2} = \exp(-bD) \quad (2)$$

where S_{b1} and S_{b2} are signal intensities at different *b*-values, which are equal to or greater than 200 s/mm².

We first obtained D with the least-squares method using Equation (2). Then, D* and f were obtained with the Nelder-Mead simplex method using Equation (1) [19] because low perfusion fraction, limited sampling, or low precision were challenging in a simultaneous nonlinear fit using Equation (1) [20].

We used a workstation (Volume analyser SYNAPSE VINCENT, FUJIFILM Corporation, Tokyo, Japan) to calculate each parameter. The regions of interest (ROIs) in the bilateral parotid, submandibular, and sublingual glands were set manually in DWI at a *b*-value of 0 s/mm² by a radiologic technologist (Figures 1 and 2). The sizes of the ROIs were 39.5, 39.5, and 23.4 mm², respectively. A single ROI was set for each salivary gland. Then, they were copied automatically in an ADC, D, D*, and f maps. The average signals in each ROI were calculated. The ROIs were set to avoid large vessels or salivary gland ducts at the maximum diameter level of the salivary gland by referring to DWI at a *b*-value of 0 s/mm² and an ADC map. ADC was calculated using the following equation:

$$S_{b1}/S_{b2} = \exp\{-(b_1 - b_2)(ADC)\} \quad (3)$$

where S_{b1} and S_{b2} are signal intensities at different *b*-values (b_1 and b_2). We obtained the ADC with the least-squares method using Equation (3).

Quantitative analysis

First, the parameters were calculated through IVIM-DWI using 13 *b*-values (the full combination) and were considered the standard values. Second, each parameter was calculated through IVIM-DWI using 10 *b*-values (10-A to 10-D combinations) selected from the full combination,

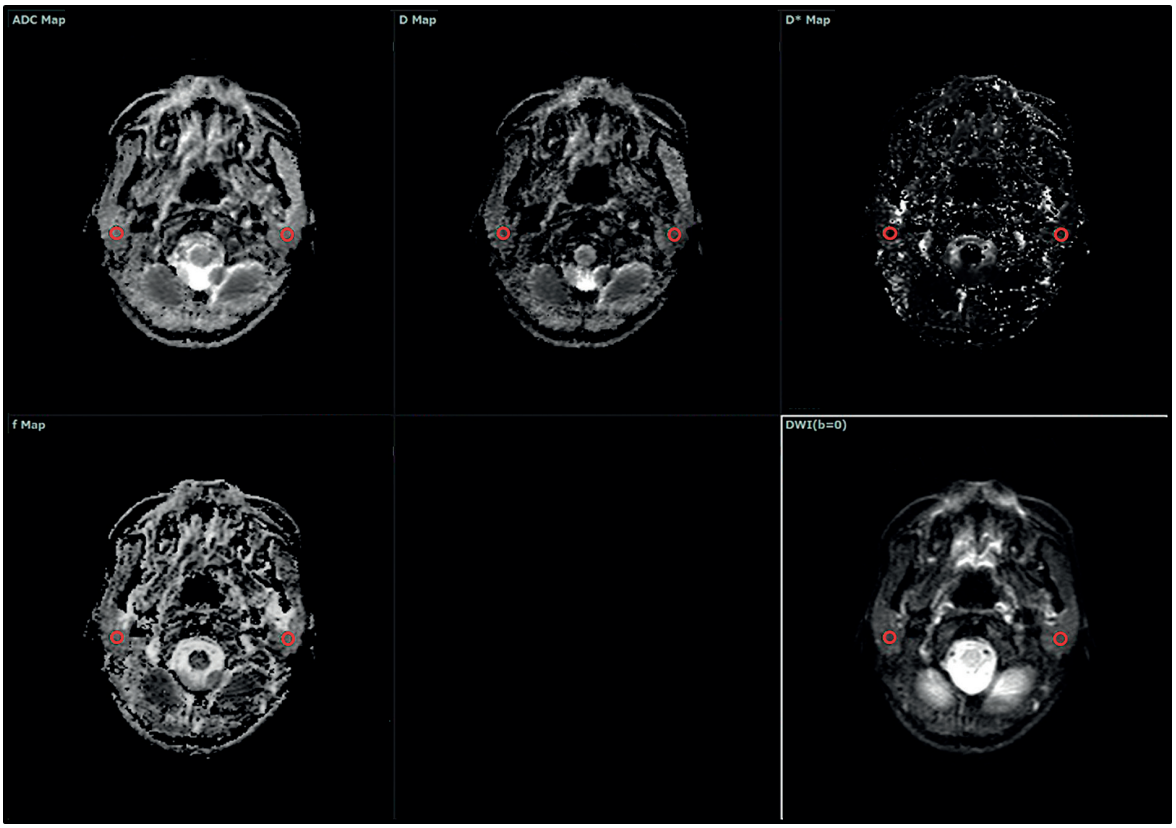

Figure 1. Regions of interest (ROIs) in an apparent diffusion coefficient (ADC) map, D map, D* map, f map, and diffusion-weighted imaging (DWI) at a *b*-value of 0 s/mm^2 in the bilateral parotid glands. A radiologic technologist manually set the ROIs in the bilateral parotid glands in DWI at a *b*-value of 0 s/mm^2. The size of the ROI is 39.5 mm^2. The ROIs were copied automatically on an ADC map, D map, D* map, and f map

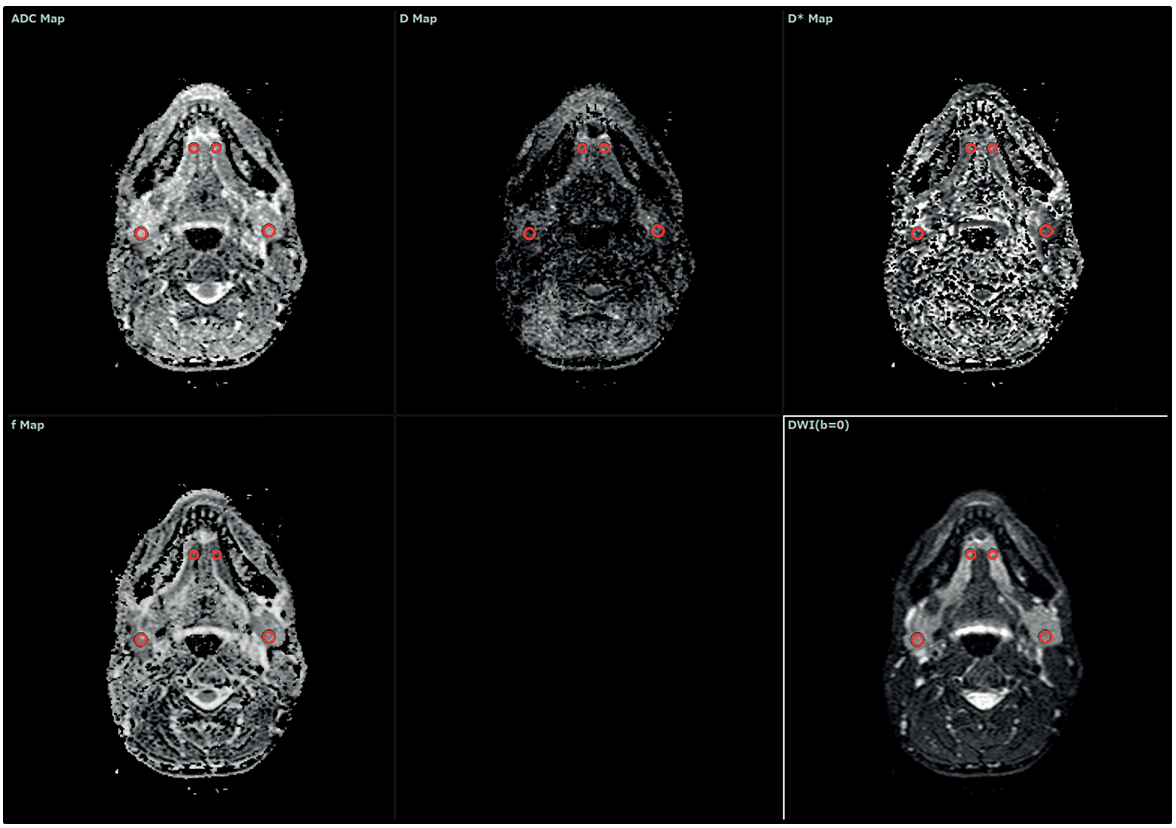

Figure 2. Regions of interest (ROIs) in an apparent diffusion coefficient map, D map, D* map, f map, and diffusion-weighted imaging (DWI) at a *b*-value of 0 s/mm^2 in the bilateral submandibular and sublingual glands. The ROIs in the bilateral submandibular and sublingual glands were set similarly to those in the bilateral parotid glands. The sizes of the ROIs are 39.5 and 23.4 mm^2, respectively

and each parameter was compared with the standard values. Table 1 shows the number and combination of *b*-values. Thereafter, combinations of 8 *b*-values were used by referring to the combinations of 10 *b*-values. Each parameter was calculated through IVIM-DWI using combinations of 8 *b*-values and was compared with the standard values. Using a similar method, the combinations of 6 and 5 *b*-values were used, and each parameter was calculated and compared with the standard values. A *b*-value of 0 s/mm^2 was included in all combinations because Equation (1) included S_0, which was the signal intensity at a *b*-value of 0 s/mm^2.

For the parameters in the full combination and the combinations of *b*-values that did not significantly differ from the standard values, we calculated the mean values of the signal intensity and standard deviations (SDs) of these parameters in the major salivary glands. When we calculated the mean values of the signal intensity and SDs, the ROIs were set manually on DWI at each *b*-value by a radiologic technologist, similarly to the evaluation of IVIM parameters and ADC. Additionally, the signal-to-noise ratio (SNR) in the major salivary glands of each *b*-value was calculated using the following equation:

$$SNR = S/SD, \quad (4)$$

where *S* is the signal intensity in each major salivary gland and *SD* is the standard deviation of the signal intensity in each major salivary gland. The signal intensity shows the mean value in the ROIs of the bilateral major salivary glands.

The bi-exponential signal decay curves in some combinations of *b*-values were obtained in the major salivary glands. These curves were obtained by substituting Equation (1) for *b*-values and mean values of IVIM parameters in the major salivary glands.

Statistical analysis

The Wilcoxon signed-rank test was used to determine whether there were any differences between the standard values and parameters assessed through IVIM-DWI using each combination ($p < 0.05$). JMP® 15 software (SAS Institute Inc., Cary, NC, USA) was used for the analysis. Moreover, we applied Bonferroni correction for multiple comparisons and set the corrected significance level to less than 0.05/4 = 0.0125.

The coefficient of variation (CV) was used to evaluate the reproducibility of ln (S_b/S_0) for each *b*-value in 10 volunteers. Moreover, it was used to evaluate the reproducibility of each parameter in the major salivary glands of 10 volunteers and was calculated using the following equation:

$$CV\ [\%] = |SD/mean| \times 100 \quad (5)$$

The CV was calculated using the mean value and SD for each parameter of 10 volunteers.

The Steel-Dwass test was used to determine whether there were any differences in each parameter in the major salivary glands ($p < 0.05$). JMP® 13 software (SAS Institute Inc., Cary, NC, USA) was used for the analysis.

Results

The number and combination of *b*-values

Table 1 shows the number and combination of *b*-values. The 8-A and 8-B combinations were obtained using the

Table 1. The number and combination of *b*-values

Combination	Low *b*-value [s/mm^2]								High *b*-value [s/mm^2]				
	0	10	20	30	40	50	75	100	200	300	500	750	1000
Full	•	•	•	•	•	•	•	•	•	•	•	•	•
10-A	•	•	•				•	•	•	•	•	•	•
10-B	•	•		•		•		•	•	•	•	•	•
10-C	•	•	•	•	•	•	•	•	•				•
10-D	•	•	•	•	•	•	•	•		•		•	
8-A	•	•	•				•	•	•	•			•
8-B	•	•	•				•	•	•		•		•
8-C	•	•		•		•		•	•	•			•
8-D	•	•		•		•		•	•		•		•
6-A	•	•					•		•		•		•
6-B	•		•					•	•		•		•
6-C	•	•				•			•		•		•
6-D	•			•				•	•		•		•
5-A	•	•							•		•		•

10-A combination because there were no significant differences between the standard values and parameters derived using IVIM-DWI with the 10-A combination. The 8-C and 8-D combinations were achieved using the 10-B combination, 6-A and 6-B combinations using the 8-B combination, 6-C and 6-D combinations using the 8-D combination, and the 5-A combination was obtained using the 6-A and 6-C combinations because there were no significant differences between the standard values and parameters derived using IVIM-DWI with the 10-B, 8-B, 8-D, and 6-A, 6-C combinations, respectively.

Quantitative analysis

Tables 2, 3, 4, and 5 demonstrate the mean values ± SD of the IVIM parameters and ADC in the bilateral major salivary glands for each combination of b-values. There were statistically significant differences between the standard values and parameters derived using IVIM-DWI with the 10-C, 10-D, 8-A, 8-C, 6-B, and 5-A combinations ($p < 0.0125$).

Table 6 shows the CV of ln (S_b/S_0) for each *b*-value in the major salivary glands. The CV of ln (S_b/S_0) at a *b*-value

Table 2. The mean values and SD of the D values [$\times 10^{-3}$ mm^2/s] in the bilateral major salivary glands of each combination

b-value	Parotid gland		Submandibular gland		Sublingual gland	
	Mean ± SD	*p*-value	Mean ± SD	*p*-value	Mean ± SD	*p*-value
Full	0.905 ± 0.268	–	1.01 ± 0.223	–	1.14 ± 0.454	–
10-A	0.908 ± 0.272	0.500	1.01 ± 0.217	0.750	1.14 ± 0.461	1.000
10-B	0.899 ± 0.264	0.188	1.01 ± 0.225	0.609	1.14 ± 0.459	0.250
10-C	0.907 ± 0.321	0.883	1.00 ± 0.276	0.877	1.09 ± 0.521	0.241
10-D	0.983 ± 0.500	0.577	1.18 ± 0.604	0.273	1.31 ± 0.660	0.186
8-A	0.878 ± 0.267	0.045	0.990 ± 0.186	0.336	1.13 ± 0.453	0.279
8-B	0.882 ± 0.314	0.641	0.958 ± 0.258	0.265	1.09 ± 0.484	0.165
8-C	0.883 ± 0.275	0.091	0.991 ± 0.193	0.213	1.13 ± 0.453	0.327
8-D	0.880 ± 0.313	0.564	0.958 ± 0.248	0.290	1.09 ± 0.484	0.165
6-A	0.880 ± 0.312	0.564	0.955 ± 0.253	0.249	1.07 ± 0.476	0.048
6-B	0.881 ± 0.314	0.589	0.955 ± 0.253	0.249	1.08 ± 0.489	0.106
6-C	0.879 ± 0.308	0.565	0.954 ± 0.256	0.249	1.11 ± 0.506	0.346
6-D	0.883 ± 0.314	0.628	0.942 ± 0.252	0.103	1.06 ± 0.477	0.049
5-A	0.880 ± 0.313	0.564	0.959 ± 0.252	0.298	1.09 ± 0.491	0.125

Table 3. The mean values and SD of the D* values [$\times 10^{-3}$ mm^2/s] in the bilateral major salivary glands of each combination

b-value	Parotid gland		Submandibular gland		Sublingual gland	
	Mean ± SD	*p*-value	Mean ± SD	*p*-value	Mean ± SD	*p*-value
Full	46.3 ± 31.7	–	46.4 ± 32.7	–	40.7 ± 28.1	–
10-A	39.9 ± 32.4	0.165	46.4 ± 28.3	0.430	32.9 ± 22.7	0.475
10-B	46.9 ± 25.7	0.564	44.9 ± 30.2	0.522	48.1 ± 30.6	0.0296
10-C	50.4 ± 29.9	0.0637	51.5 ± 32.8	0.294	42.1 ± 24.5	0.546
10-D	30.5 ± 25.4	< 0.0001*	39.2 ± 25.2	0.165	27.6 ± 23.3	0.0012*
8-A	38.6 ± 31.4	0.143	51.2 ± 31.1	0.729	32.1 ± 23.7	0.261
8-B	41.6 ± 31.4	0.277	52.2 ± 31.9	0.622	34.7 ± 22.1	0.143
8-C	47.1 ± 26.0	0.498	47.3 ± 31.6	0.674	43.5 ± 26.9	0.277
8-D	48.6 ± 21.7	0.522	44.5 ± 28.3	0.956	47.8 ± 24.9	0.165
6-A	35.8 ± 13.4	0.409	42.2 ± 18.7	0.701	37.8 ± 22.3	0.956
6-B	34.1 ± 34.6	0.0094*	43.5 ± 33.2	0.546	29.8 ± 26.8	0.105
6-C	43.9 ± 19.1	0.756	49.3 ± 25.8	0.596	43.3 ± 24.4	0.246
6-D	33.2 ± 29.2	0.0583	30.9 ± 28.5	0.0172	35.7 ± 33.0	0.349
5-A	37.2 ± 16.1	0.294	50.1 ± 21.7	0.784	35.2 ± 34.4	0.648

*Bonferroni-adjusted *p*-values < 0.0125 at multivariate analysis.

Table 4. The mean values and SD of the f values [%] in the bilateral major salivary glands of each combination

b-value	Parotid gland		Submandibular gland		Sublingual gland	
	Mean ± SD	*p*-value	Mean ± SD	*p*-value	Mean ± SD	*p*-value
Full	34.5 ± 15.5	–	45.3 ± 14.9	–	34.0 ± 20.2	–
10-A	31.8 ± 17.1	0.0710	44.3 ± 15.2	0.107	32.9 ± 18.6	0.354
10-B	35.2 ± 16.2	0.459	45.5 ± 14.2	0.257	34.5 ± 19.7	0.774
10-C	31.6 ± 16.9	0.185	45.5 ± 14.8	0.552	37.6 ± 18.6	0.299
10-D	38.0 ± 18.1	0.0328	47.2 ± 18.4	0.528	43.9 ± 18.4	0.0022*
8-A	32.1 ± 17.6	0.0894	42.5 ± 16.3	0.334	34.6 ± 19.6	0.307
8-B	32.2 ± 16.0	0.0799	46.1 ± 14.3	0.819	34.1 ± 19.1	0.906
8-C	34.6 ± 16.9	0.195	45.2 ± 15.1	0.602	38.6 ± 18.6	0.013
8-D	36.4 ± 15.1	0.0935	48.8 ± 13.9	0.168	38.0 ± 21.0	0.363
6-A	31.1 ± 14.5	0.0371	46.3 ± 13.6	0.978	33.2 ± 19.9	0.672
6-B	33.3 ± 15.7	0.630	46.9 ± 14.0	0.504	34.2 ± 18.3	0.589
6-C	33.8 ± 14.6	0.481	46.5 ± 13.1	0.701	38.4 ± 20.3	0.354
6-D	34.0 ± 13.6	0.414	48.7 ± 11.1	0.281	33.8 ± 16.2	0.763
5-A	30.3 ± 14.9	0.0075*	45.9 ± 14.3	0.841	31.5 ± 19.6	0.784

*Bonferroni-adjusted *p*-values < 0.0125 at multivariate analysis.

Table 5. The mean values and SD of the ADC values [$\times 10^{-3}$ mm^2/s] in the bilateral major salivary glands of each combination

b-value	Parotid gland		Submandibular gland		Sublingual gland	
	Mean ± SD	*p*-value	Mean ± SD	*p*-value	Mean ± SD	*p*-value
Full	1.07 ± 0.357	–	1.45 ± 0.346	–	1.25 ± 0.539	–
10-A	1.08 ± 0.405	0.383	1.44 ± 0.387	0.945	1.27 ± 0.608	0.798
10-B	1.05 ± 0.357	0.297	1.42 ± 0.358	0.0808	1.24 ± 0.556	0.317
10-C	1.00 ± 0.332	0.0038*	1.34 ± 0.288	<.0001*	1.22 ± 0.491	0.057
10-D	1.18 ± 0.444	0.0016*	1.62 ± 0.515	0.0022*	1.34 ± 0.620	0.028
8-A	1.03 ± 0.400	0.234	1.36 ± 0.349	0.0016*	1.24 ± 0.586	0.534
8-B	1.07 ± 0.413	0.746	1.43 ± 0.371	0.561	1.27 ± 0.615	0.805
8-C	1.01 ± 0.361	0.0090*	1.35 ± 0.321	<.0001*	1.21 ± 0.535	0.045
8-D	1.05 ± 0.365	0.136	1.41 ± 0.339	0.145	1.24 ± 0.557	0.325
6-A	1.12 ± 0.423	0.0973	1.47 ± 0.376	0.447	1.31 ± 0.616	0.199
6-B	1.03 ± 0.397	0.186	1.37 ± 0.363	0.0044*	1.24 ± 0.623	0.509
6-C	1.08 ± 0.403	0.576	1.44 ± 0.377	0.777	1.28 ± 0.608	0.588
6-D	1.04 ± 0.349	0.0816	1.38 ± 0.313	0.03	1.23 ± 0.530	0.701
5-A	1.14 ± 0.466	0.121	1.49 ± 0.425	0.307	1.33 ± 0.684	0.245

* Bonferroni-adjusted *p*-values < 0.0125 at multivariate analysis.

of 10 s/mm^2 was the lowest among the low *b*-values, and that for a *b*-value of 300 s/mm^2 was the highest among the high *b*-values in all the major salivary glands. Figure 3 presents the mean values and SD of the IVIM parameters and ADC in the major salivary glands, and Table 7 depicts their CV. There were statistically significant differences in IVIM parameters in some pairs of major salivary glands ($p < 0.05$). The f values for the submandibular gland in Figure 3 were significantly higher than the those for the other 2 glands. The CV in D, D*, f, and ADC values were 25.0-43.1%, 64.0-67.0%, 30.0-56.0%, and 25.2-46.0%, respectively, in the major salivary glands. Table 8 shows the SNR in the major salivary glands for each *b*-value. The average SNR of each *b*-value in the major salivary glands was 6.04-10.2.

The signal decay curves

Figure 4 shows the bi-exponential signal decay curves obtained from the full combination and the 6-A and 6-C

Table 6. The CV of ln (S_b/S_0) for each *b*-value

b-value [s/mm²]	The CV [%] of ln (S_b/S_0)			
	Parotid gland	Submandibular gland	Sublingual gland	All the major salivary glands
0	NA	NA	NA	NA
10	31.5	40.3	84.7	57.9
20	94.1	63.4	130	92.6
30	173	129	234	173
40	160	141	179	159
50	103	81.1	132	107
75	126	88.7	136	116
100	78.9	68.1	81.4	76.3
200	65.0	38.5	70.5	59.8
300	76.5	57.0	98.4	77.1
500	47.6	36.3	66.9	52.3
750	39.3	34.5	52.8	44.2
1000	38.2	27.2	49.0	40.1

NA – not applicable.

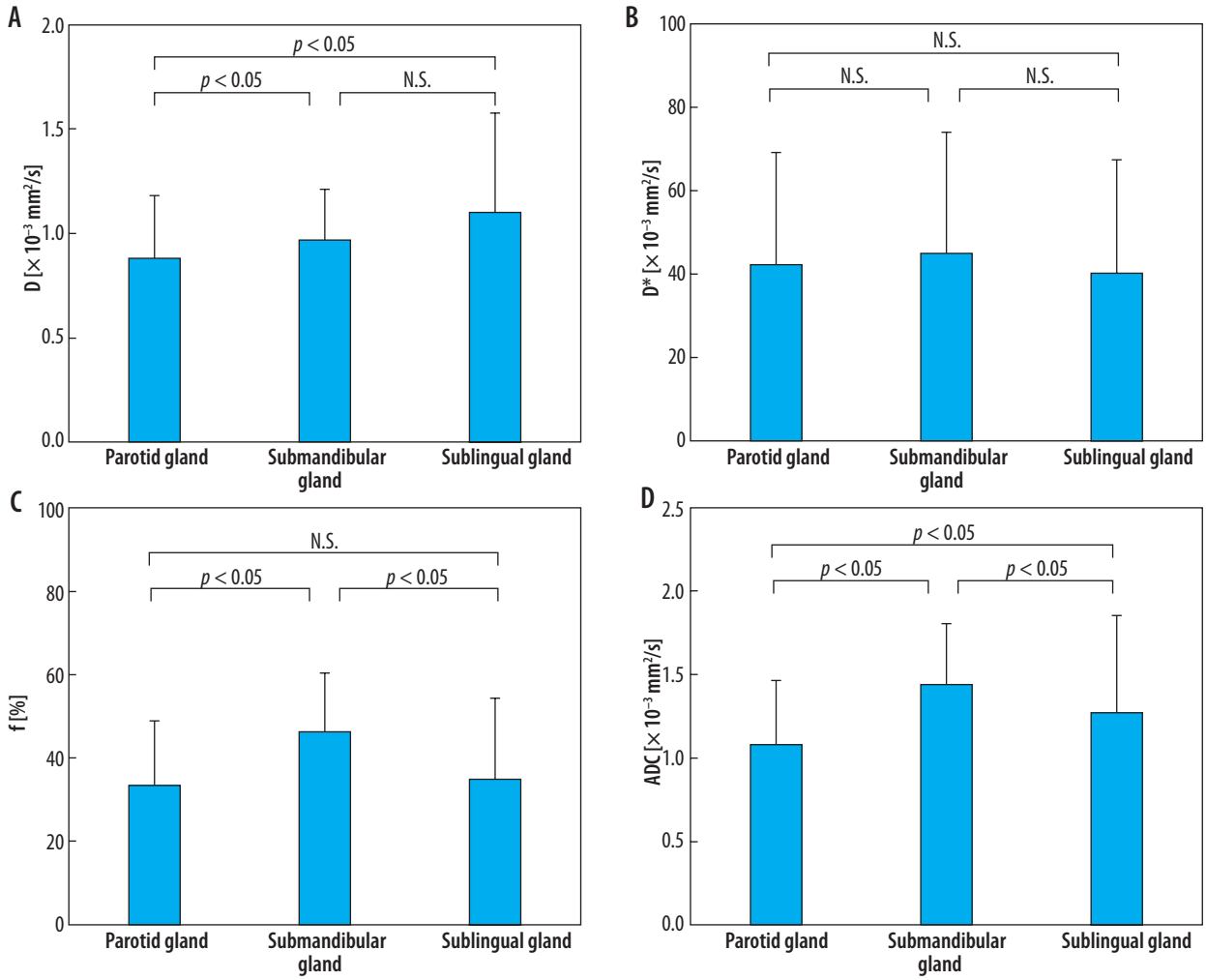

Figure 3. Mean values and standard deviation (SD) of the intravoxel incoherent motion (IVIM) parameters and apparent diffusion coefficient (ADC) in the major salivary glands. There were statistically significant differences in IVIM parameters and ADC in some pairs of the major salivary glands ($p < 0.05$)

Table 7. The CV of IVIM parameters and ADC in the bilateral major salivary glands

	Parotid gland	Submandibular gland	Sublingual gland
The CV [%] of D values	33.4	25.0	43.1
The CV [%] of D* values	64.0	64.9	67.0
The CV [%] of f values	45.9	30.0	56.0
The CV [%] of ADC values	36.0	25.2	46.0

combinations in the major salivary glands. There were few differences between the bi-exponential signal decay curves obtained from the full combination and the 6-A and 6-C combinations.

Discussion

Our study showed that the number of *b*-values could be reduced to a minimum of 6 in IVIM-DWI of the major salivary glands. Moreover, they should include 3 low and 3 high *b*-values. This result was based on the fact that there were no significant differences between the standard values and parameters derived using IVIM-DWI with either the 6-A or 6-C combination. Conversely, there were statistically significant differences between the standard values and parameters derived using IVIM-DWI with the 5-A combination, which included 2 low *b*-values, and the 10-C and 10-D combinations, which included 2 high *b*-values. Based on the combinations of *b*-values with a statistically significant difference in the parameters compared with the standard values, we believe that IVIM-DWI using 5 or fewer *b*-value combinations should have demonstrated a significant difference from the standard values, and we believe that it is possible that IVIM-DWI of the major salivary glands could be performed using 3 low and 3 high *b*-values at the lowest. Additionally, Figure 4 shows few differences between the bi-exponential signal decay curves obtained from the full combination and the 6-A and 6-C combinations in the major salivary glands. Moreover, the imaging time of IVIM-DWI with 6 *b*-values such as the 6-A or 6-C combination was about a half of that with 13 *b*-values (full); therefore, less motion artefact of IVIM-DWI with 6 *b*-values could be expected to occur compared with that with 13 *b*-values (full). This needs to be validated in future studies [8]. Therefore, we believe that it is possible that IVIM-DWI of the major salivary glands could be performed using 3 low and 3 high *b*-values.

The CV of ln (S_b/S_0) at a *b*-value of 10 s/mm^2 was the lowest among the low *b*-values in all the major salivary glands, and we speculated that there was less difference in the bi-exponential curve fitting between the combinations with a *b*-value of 10 s/mm^2 and full. Thus, there were no significant differences between the standard values and parameters derived using IVIM-DWI with 3 low *b*-values, which included a *b*-value of 10 s/mm^2. The CV of ln (S_b/S_0) at a *b*-value of 300 s/mm^2 was the highest among the high *b*-values in all the major salivary glands, and we speculated that there were large differences in the bi-exponential curve fitting between the combinations with a *b*-value of 300 s/mm^2 and full. Therefore, there were statistically significant differences between the standard values and parameters derived using IVIM-DWI with 3 high *b*-values, which included a *b*-value of 300 s/mm^2. Moreover, the CV of ln (S_b/S_0) in all *b*-values was high (27.2-234%); therefore, we speculated that there could be differences in the bi-exponential curve fitting between the combinations of 10-C with 2 high *b*-values, 5-A with 2 low *b*-values, and full.

Table 8. The SNR in the major salivary glands for each *b*-value

b-value [s/mm^2]	SNR of parotid gland Mean ± SD	SNR of submandibular gland Mean ± SD	SNR of sublingual gland Mean ± SD	Mean ± SD
0	8.84 ± 2.39	10.6 ± 1.98	10.1 ± 2.98	9.86 ± 2.59
10	10.6 ± 2.49	9.34 ± 3.26	10.7 ± 5.08	10.2 ± 3.82
20	10.2 ± 2.37	8.22 ± 2.62	10.1 ± 4.04	9.50 ± 3.23
30	10.4 ± 3.04	8.63 ± 2.33	9.50 ± 4.67	9.50 ± 3.56
40	10.6 ± 3.47	8.27 ± 2.72	7.09 ± 3.90	8.64 ± 3.69
50	10.2 ± 2.96	8.70 ± 4.24	7.78 ± 4.81	8.88 ± 4.19
75	10.3 ± 3.46	8.53 ± 3.26	7.09 ± 4.08	8.65 ± 3.85
100	9.96 ± 3.40	8.59 ± 4.14	7.26 ± 4.51	8.60 ± 4.19
200	9.72 ± 2.87	6.40 ± 2.01	8.28 ± 4.59	8.13 ± 3.60
300	9.90 ± 2.85	6.58 ± 2.41	8.28 ± 4.85	8.25 ± 3.78
500	8.31 ± 3.03	5.60 ± 1.16	7.52 ± 3.94	7.15 ± 3.16
750	7.12 ± 1.77	5.68 ± 1.35	6.00 ± 2.67	6.27 ± 2.10
1000	6.94 ± 1.81	4.78 ± 0.74	6.39 ± 3.27	6.04 ± 2.38

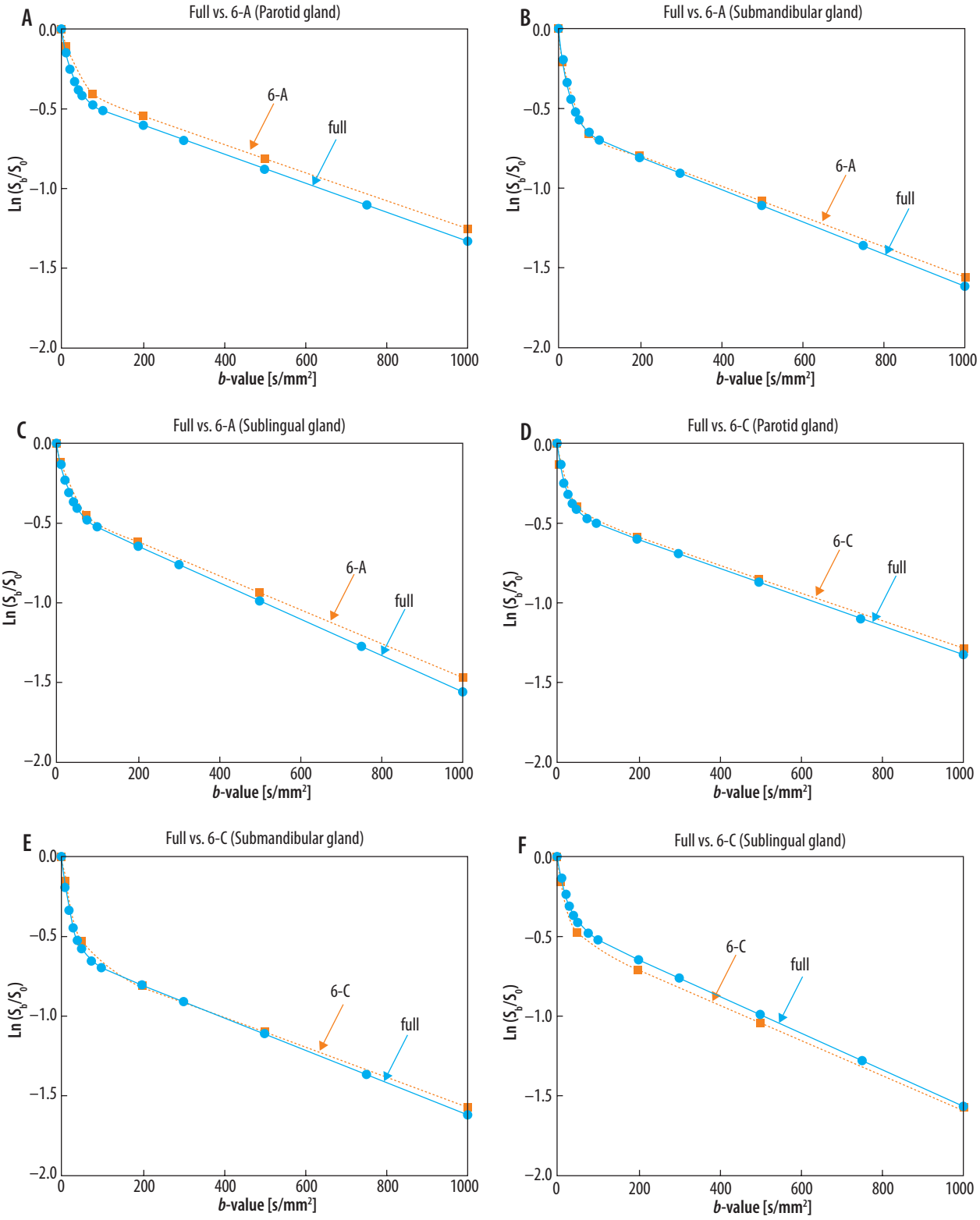

Figure 4. The bi-exponentially signal decay curves obtained from the full combination and the 6-A and 6-C combinations in the major salivary glands. There were few differences between the bi-exponential signal decay curves obtained from the full and 6-A and 6-C combinations

Figure 3 shows that statistically significant differences were observed in the parameters in some pairs of the major salivary glands. The parotid sublingual, and submandibular glands are serous, mucus, and mixed types of serous and mucus glands, respectively. Thus, the histological difference might have caused statistically significant differences in the parameters of the major salivary glands.

The f values for the submandibular gland in Figure 3 were significantly higher than those for the other 2 glands, and the CV of D, D*, f, and ADC values in the major salivary glands were high in Table 7 (25.0-43.1%, 64.0-67.0%, 30.0-56.0%, and 25.2-46.0%, respectively). Additionally, the average SNR of each *b*-value was 6.04-10.2 in our study, which was almost similar to the critical SNR

reported in a previous study on *b*-values of IVIM-DWI optimized using Monte-Carlo simulations [3]. Moreover, Verhappen *et al*. or Mikayama *et al*. reported that the susceptibility artefacts of EPI-DWI derived using magnetic inhomogeneity cause image distortion in the head and neck, and they may inhibit obtaining accurate measurements of IVIM parameters and ADC [18,21]. Furthermore, the submandibular glands or the organs in proximity to the airway or jaw might be more sensitive to motion artefacts for respirating or swallowing [22]. Slightly low SNR, susceptibility artefacts, and motion artefacts might have affected the measurement of each parameter in this study. Thus, we speculated that the f values for the submandibular gland were significantly higher than those for the other 2 glands, and the CV of D, D*, f, and ADC values in the major salivary glands were high.

This study has several limitations. First, our study only included young and normal volunteers, and the presence of salivary gland tumours was not investigated. Second, our study population was relatively small. Thus, future studies with several volunteers and patients, including both young and elderly individuals, should be conducted. Third, EPI-DWI was used in the IVIM-DWI of this study. We suspect that distorted images due to magnetic inhomogeneity around the major salivary glands in EPI-DWI affected the IVIM parameters and ADC in this study. Hence, future studies using an imaging method such as turbo spin echo (TSE)-DWI, which can cause few susceptibility artefacts or minimal distortion in IVIM-DWI, can improve the evaluation of each parameter of the major salivary glands.

Conclusions

IVIM-DWI of the major salivary glands could be performed using a minimum of 6 *b*-values. However, they should contain 3 low and 3 high *b*-values. Moreover, patients could benefit from shortening the time in IVIM-DWI of the major salivary glands.

Conflicts of interest

The authors report no conflict of interest.

References

1. Le Bihan D, Breton E, Lallemand D, et al. MR imaging of intravoxel incoherent motions: application to diffusion and perfusion in neurological disorders. Radiology 1986; 161: 401-407.
2. Le Bihan D, Breton E, Lallemand D, et al. Separation of diffusion and perfusion in intravoxel incoherent motion MR imaging. Radiology 1988; 168: 497-505.
3. Lemke A, Stieltjes B, Schad LR, Laun FB. Toward an optimal distribution of b values for intravoxel incoherent motion imaging. Magn Reson Imaging 2011; 29: 766-776.
4. Zhang JL, Sigmund EE, Rusinek H, et al. Optimization of b-value sampling for diffusion-weighted imaging of the kidney. Magn Reson Med 2012; 67: 89-97.
5. Pang Y, Turkbey B, Bernardo M, et al. Intravoxel incoherent motion MR imaging for prostate cancer: an evaluation of perfusion fraction and diffusion coefficient derived from different b-value combinations. Magn Reson Med 2013; 69: 553-562.
6. Cho GY, Moy L, Zhang JL, et al. Comparison of fitting methods and b-value sampling strategies for intravoxel incoherent motion in breast cancer. Magn Reson Med 2015; 74: 1077-1085.
7. Cohen AD, Schieke MC, Hohenwalter MD, Schmainda KM. The effect of low b-values on the intravoxel incoherent motion derived pseudodiffusion parameter in liver. Magn Reson Med 2015; 73: 306-311.
8. Dyvorne H, Jajamovich G, Kakite S, et al. Intravoxel incoherent motion diffusion imaging of the liver: optimal b-value subsampling and impact on parameter precision and reproducibility. Eur J Radiol 2014; 83: 2109-2113.
9. Sumi M, Van Cauteren M, Sumi T, et al. Salivary gland tumors: use of intravoxel incoherent motion MR imaging for assessment of diffusion and perfusion for the differentiation of benign from malignant tumors. Radiology 2012; 263: 770-777.
10. Sumi M, Nakamura T. Head and neck tumors: assessment of perfusion–related parameters and diffusion coefficients based on the intravoxel incoherent motion model. AJNR Am J Neuroradiol 2013; 34: 410-416.
11. Hauser T, Essig M, Jensen A, et al. Characterization and therapy monitoring of head and neck carcinomas using diffusion-based intravoxel incoherent motion parameters – preliminary results. Neuroradiology 2013; 55: 527-536.
12. Hauser T, Essig M, Jensen A, et al. Prediction of treatment response in head and neck carcinomas using IVIM-DWI: Evaluation of lymph node metastasis. Eur J Radiol 2014; 83: 783-787.
13. Marzi S, Piludu F, Vidiri A. Assessment of diffusion parameters by intravoxel incoherent motion MRI in head and neck squamous cell carcinoma. NMR Biomed 2013; 26: 1806-1814.
14. Xu XQ, Choi YJ, Sung YS, et al. Intravoxel incoherent motion MR imaging in the head and neck: correlation with dynamic contrast-enhanced MR imaging and diffusion-weighted imaging. Korean J Radiol 2016; 17: 641-649.
15. Marzi S, Forina C, Marucci L, et al. Early radiation-induced changes evaluated by intravoxel incoherent motion in the major salivary glands. J Magn Reson Imaging 2015; 41: 974-982.
16. Hejduk B, Bobek-Billewicz B, Rutkowski T, et al. Application of Intravoxel Incoherent Motion (IVIM) Model for Differentiation Between Metastatic and Non-Metastatic Head and Neck Lymph Nodes. Pol J Radiol 2017; 82: 506-510.
17. Noij DP, Martens RM, Marcus JT, et al. Intravoxel incoherent motion magnetic resonance imaging in head and neck cancer: a systematic

review of the diagnostic and prognostic value. Oral Oncol 2017; 68: 81-91.
18. Verhappen MH, Pouwels PJ, Ljumanovic R, et al. Diffusion-weighted MR imaging in head and neck cancer: comparison between half-fourier acquisition single-shot turbo spin-echo and EPI techniques. AJNR 2012; 33: 1239-1246.
19. Patel J, Sigmund EE, Rusinek H, et al. Diagnosis of cirrhosis with intravoxel incoherent motion diffusion MRI and dynamic contrast-enhanced MRI alone and in combination: preliminary experience. J Magn Reson Imaging 2010; 31: 589-600.
20. Istratov AA, Vyvenko OF. Exponential analysis in physical phenomena. Rev Sci Instrum 1999; 70: 1233-1257.
21. Mikayama R, Yabuuchi H, Sonoda S, et al. Comparison of intravoxel incoherent motion diffusion-weighted imaging between turbo spin-echo and echo-planar imaging of the head and neck. Eur Radiol 2018; 26: 316-324.
22. Szubert-Franczak AE, Naduk-Ostrowska M, Pasicz K, et al. Intravoxel incoherent motion magnetic resonance imaging: basic principles and clinical applications. Pol J Radiol 2020; 85: e624-635.